Article

Journal of
Nanoscience and Nanotechnology
Vol. 18, 1–7, 2018
www.aspbs.com/jnn

Chemisorption of H_2S on Copper-ETS-2: Experiment and Modeling of a Packed Column

Sabereh Rezaei[1], Adolfo M. Avila[2], and Steven M. Kuznicki[1,*]

[1] *Department of Chemical and Materials Engineering, University of Alberta, Edmonton, Alberta T6G 2V4, Canada*
[2] *INQUINOA, Universidad Nacional de Tucumán, CONICET, DIPyGI-FACET-UNT, Av. Independencia 1800, C.P. 4000 San Miguel de Tucumán, Argentina*

Copper supported on Engelhard Titanosilicate-2 (ETS-2) showed to be a promising adsorbent for deep H_2S removal (to sub-ppm levels) for gas purification applications at room temperature. Because of the high external surface area and the cation exchange capacity of ETS-2, Cu ions are highly dispersed and very accessible to H_2S molecules. In this study, H_2S column breakthrough experiments are analyzed by a dynamic model based on the rigorous mass balance equations applied to the fixed-bed. The proposed model also includes the chemical reaction term, which is affected by the deactivation of the solid phase. Temperature-programmed desorption tests provided insight on the material characterization as well as on the relative magnitudes of the H_2S-material interactions.

Keywords: Chemisorption, Copper Nano-Titanate ETS-2, H_2S Breakthrough, Transport Equation.

1. INTRODUCTION

Sulfidation reactions between metal oxides and H_2S are widely applied in the industrial H_2S removal plants in wide range of working temperatures.[1–6] At room temperature, high surface area materials such as zeolites,[7–9] carbon sorbents,[10,11] mesoporous and silica material[8,12–15] are frequently used as supports to load metal/metal oxides and improve H_2S uptake by high dispersion of active sites. Recently, a unique titanosilicate material (ETS-2) was synthesized and loaded with Cu active sites, Cu-ETS-2, for deep H_2S removal (to sub-ppm levels) for gas purification applications at room temperature.[16,17] Cu-ETS-2 displayed the most promising adsorbent in comparison to a fully developed commercial H_2S adsorbent and other tested metal-exchanged ETS-2. Also, Cu-ETS-2 has the chemical environment favorable for decomposition of H_2S. Since it has been shown that a transition-metal ion,[18–23] metal oxides[24] and TiO_2 surface[25] enhance H_2S adsorption by facilitating its dissociation to HS^- and S^- ions, which may further react and form sulfide products.[26]

Although several studies focused on the development of H_2S sorbents at low temperatures and measurements of the breakthrough curves, the column dynamics are still poorly understood and differ for many of the sorbents studied. Much progress has been made for the column dynamics and interactions of gases with physisorbents without any chemical reaction included[27–30] and less attention to chemisorption and surface reactions.[31] For H_2S compound less attention was paid to the investigation of the adsorbent by a dynamic model, which considers both chemisorption of H_2S molecules on the surface and deactivation of the solid.

In general, textural variations of solid reactants, changes in active surface area, reactivity of the solid and formation of a dense product layer over the solid reactant cause a significant decrease in activity of the solid reactant during reaction.[32,33] Deactivation models[34,35] were reported to predict the reaction rates of such gas–solid non-catalytic reactions. However, the models were considering pseudo-steady state conditions[36–42] in which the dynamic deactivation is included in the activity term implicitly.

The objective of this work is to gain a better understanding of the transport phenomena occurring during the adsorption of ppm level H_2S on a copper-ETS-2 packed bed column. Breakthrough adsorption experiments at room and higher temperatures (up to 250 °C) were performed.

*Author to whom correspondence should be addressed.

A continuum mechanics-based model was developed to support the analysis of experimental data obtained from dynamic column breakthrough tests. The model includes the chemical reaction term, which is affected by the deactivation of the solid phase. Temperature-programmed desorption (TPD)[43–46] experiments of H_2S on Cu-ETS-2 provided a further insight of the different H_2S-material interaction energy levels.

2. EXPERIMENTAL DETAILS

2.1. Materials

Synthesis of ETS-2 and the ion exchange procedure to make Cu-ETS-2 were followed as explained previously.[17] The final solid powder was pressed into a binderless dense disk and then crushed and sieved with the 0.297 mm to 0.595 mm (No. 30 to 50 mesh) fraction for use in the column dynamic sulfidation test experiments.

2.2. Adsorption Tests

Figure 1 shows a process flow diagram of the experimental setup for the H_2S breakthrough tests. The adsorption experiment was carried out by flowing a certified H_2S +He gas mixture (Praxair) of known composition (10 ppm H_2S) through the packed bed at different temperatures. The feed gas inlet flow rate was set up at 100 sccm by using a mass flow controller (MFC, scaled for 0–700 cc/min gas flows, Alicat Scientific). Packed-bed properties and test conditions are given in Table I.

The bed exit gas stream was sent to a gas chromatograph (GC) equipped with MXT-1 column (Restek) and a FPD detector to determine the H_2S concentration.[16] The H_2S mole fraction, $y(t)$, in the column exit was recorded as a function of time until the effluent gas H_2S composition approached the column inlet y_{in} (H_2S breakthrough profiles). Blank correction was neglected due to the prompt H_2S response for the empty column including glass wool.

Table I. Packed-bed properties and operation conditions.

Packed-bed	
Adsorbent weight [mg]	$w = 30$
Bed internal diameter [cm]	$d_b = 0.38$
Bed void fraction	$\varepsilon_b = 0.37$
Packed bed density [g/cm^3]	$\rho_b = 1.1$
Operation condition	
Temperature [°C]	$T = 25$, 150 and 250
Pressure [kPa]	$P = 101.3$
Gas flowrate [standard[a] cm^3/min]	$Q = 100$

Note: [a]25 °C and 101.3 kPa.

The spent column was then purged by flowing inert He (purity: 99.995%, Praxair) through it and simultaneously was heated at the rate ($\beta = 10$ °C/min) up to 500 °C in order to facilitate the desorption of H_2S molecules. Then it was cooled to near-ambient temperature. For the temperature program, the packed column was heated externally with a tube furnace (Barnstead Thermolyne-21100) attached with 4836-Temperature controller (Parr Instrument Company, USA). Another *K*-type thermocouple was also inserted inside the tubes to monitor the temperature at the column exit.

The entire tubing from H_2S cylinder to GC was made of Sulfinert tubes (Restek) to prevent any sulfidation on the tubing. Flow rate of the GC exit gas was measured using a bubble flow meter. In order to assure safe laboratory experiments the whole experimental set-up was located inside the fume hood.

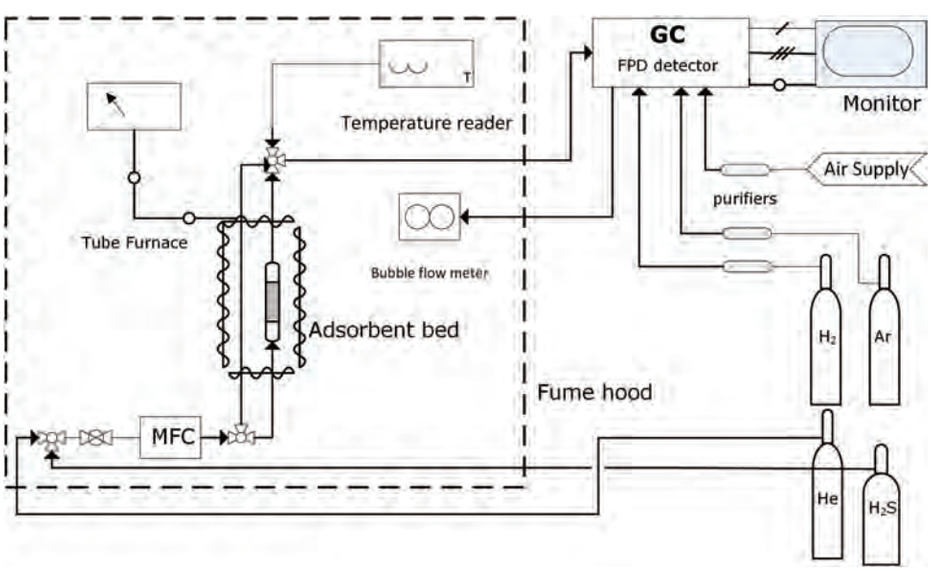

Figure 1. Schematic flow diagram of test apparatus.

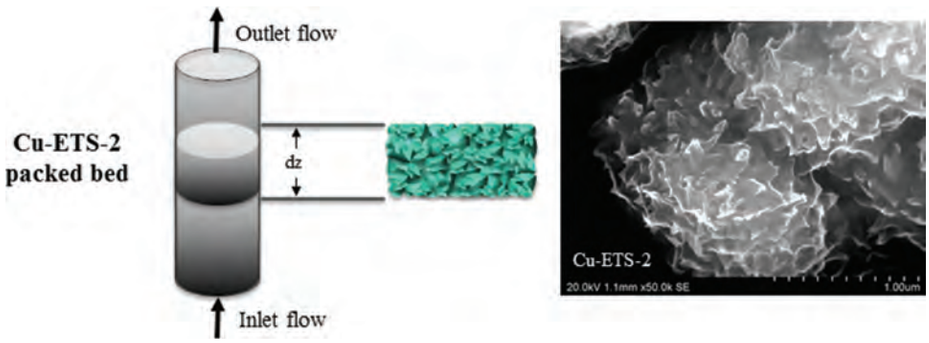

Figure 2. Illustrating image of a diluted H_2S flowing through a packed bed column of copper-ETS-2 including SEM image of Cu-ETS-2. SEM image Reprinted with permission from [17], S. Rezaei, et al., *Chem. Engi. Sci.* 123, 444 **(2015)**. © 2017, Elsevier.

3. MASS TRANSPORT MODEL FOR THE H_2S BREAKTHROUGH SIMULATION

3.1. System Modeling

Figure 2 shows a schematic of the system for modeling, which is basically described as a diluted H_2S stream flowing through a packed bed column of copper-ETS-2 adsorbent material. For the modeling of H_2S adsorption by a packed-bed of copper-ETS-2, reasonable assumptions were made, as follows:

(1) One dimensional model. Concentration gradient along the axial direction of the bed was considered.
(2) Negligible axial dispersion effects.
(3) Ideal gas law was valid in a gas stream of very low concentration of H_2S in He (10 ppm) at the experimental conditions.
(4) No heat effects were considered. Heat effects associated with adsorption and reaction can be considered negligible in a dilute adsorption regime.
(5) The pressure drop along the bed was negligible. The pressure drop calculated based on Darcy's law ($dp/dt = 150(1-\varepsilon_b)^2\mu g v/\varepsilon_b^2 d_p^2$) was less than 1%.[47]
(6) Mass transfer resistance in the gas phase was negligible.

With these assumptions, the continuity equation[48] applied within the packed-bed for H_2S species (i subscript) can be expressed as:

$$\varepsilon_b \frac{\partial c_i}{\partial t} + \varepsilon_b \nabla(c_i v) + \rho_b \frac{\partial q_i}{\partial t} = 0 \tag{1}$$

where c_i is the H_2S concentration in the gas phase [mol/cm^3] and q_i is the H_2S adsorbed in the solid phase [mol/g]. v is the interstitial velocity which remains essentially constant at low H_2S level and can be taken out of the divergence. ρ_b is the bed density [g/cm^3].

In the interaction associated with H_2S removal by the sorbent Cu-ETS-2, two sequential steps were assumed to occur.

First, molecules from the gas adsorbs on the copper site (of an energetically homogeneous sorbent) reversibly:

$$\frac{\partial C_s}{\partial t} = -K_f C_s[1-\theta] + K_b\theta \tag{2}$$

where parameters K_f and K_b represent the specific rate constants for the forward and backward chemisorption reaction, respectively, and θ represents the fraction of the sorption sites on the chemisorbent that are occupied by the chemisorbed H_2S molecules at time t ($\theta = q_i/q_i^{sat}$). At equilibrium, the reaction kinetic rate for the first step is equal to zero, which describes the Langmuirian mechanism of chemisorption:[31]

$$\theta = \frac{bc_i}{1+bc_i} \tag{3}$$

where b is the ratio of the specific rate constants for the forward and backward chemisorption reactions. When the H_2S concentration gradient in the gas phase (C_s) is negligible, the H_2S gas phase concentration near the solid phase (close to the interphase) can be considered essentially the same as that one in the bulk gas phase (c_i).

At low H_2S concentrations, the Langmuir isotherm model Eq. (2) is in the linear form of Henry's equilibrium as follows:

$$q_i = k_H c_i \tag{4}$$

Then, Eq. (1) can be rewritten as:

$$(\varepsilon_b + \rho_b k_H)\frac{\partial c_i}{\partial t} + \varepsilon_b v \frac{\partial c_i}{\partial z} = 0 \tag{5}$$

Equation (5) represents a linear adsorption model in a fixed bed and the mathematical expression is commonly known as "The Transport Equation."[47,48] This equation and its solution will be used as a reference point to better understand the experimental data.

Since many reports indicated the existence of sulfidation reaction of the chemisorbed H_2S particles on the surface,[47,48] a second step is considered here for the consumption of H_2S molecules due to surface reactions in the adsorbed phase. This can be expressed as the following kinetic expression:

$$r_i = -k_r q_i a \tag{6}$$

where k_r is the kinetic rate constant.

Equation (6) considers a deactivation rate term a that takes into account the change in the surface area and activity of the solid reactant because of the decomposed H_2S on the surface or further potential of the sulfidation reaction.[31, 32] Then, the overall effect of all these factors on the kinetic rate is expressed by the variation of an activity term introduced into the rate expression.

Taking into account the existence of chemical reaction, the continuity equation applied in the fixed-bed can be reformulated as:

$$(\varepsilon_b + \rho_b k_H)\frac{\partial c_i}{\partial t} + \varepsilon_b v \frac{\partial c_i}{\partial z} = \rho_b r_i \tag{7}$$

This equation means that any change in the H_2S concentration is associated with the convective mass transport along the bed and the surface interactions in the adsorbed phase.

In this work, the change of surface activity and solid reactant consumption with time is considered proportional to the activity and species concentration as follows:[33, 34]

$$\frac{da}{dt} = -k_d c_i a \tag{8}$$

where k_d is the deactivation constant. Using Eqs. (4), (6) and (7) the problem to solve is defined through the following PDE equation with the corresponding initial and boundary conditions:

$$(\varepsilon_b + k_H)\frac{\partial c_i}{\partial t} + \varepsilon_b v \frac{\partial c_i}{\partial z} = \rho_b K c_i a$$
$$@ \begin{cases} t = 0 & c_i = 0 \quad \text{for all } z \\ z = 0 & c_i = c_i^o \quad \text{for } t > 0 \end{cases} \tag{9}$$

where K is defined as a kinetics parameter (includes the product of the reaction rate k_r and Henry's constants $k_H \cdot c_i^o$) representing the H_2S concentration in the column inlet.

3.2. Numerical Resolution

A numerical method is used to replace the spatial derivatives with an algebraic approximation. This effectively removes the derivatives from the partial differential Eq. (9) and reduces to a system of ordinary differential equations (ODEs). Then this system of ODEs and Eq. (8) can be integrated simultaneously by standard and well-established numerical algorithms for initial value ODEs (ode15s in MATLAB_R2013a). Then an optimization function (fminsearch) is used to minimize the error between the breakthrough model and experimental breakthrough curves.

3.3. Results and Discussion

3.3.1. H_2S Breakthrough Concentration Profiles on Cu-ETS-2

Figure 3 shows the H_2S breakthrough experimental results at different temperatures (25 °C, 100 °C and 250 °C).

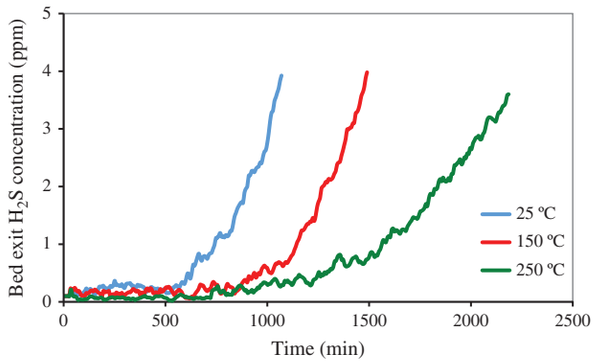

Figure 3. H_2S breakthrough curves for Cu-ETS-2 at 25 °C, 150 °C and 250 °C.

The profiles corresponding to the fixed-bed experiments performed at higher temperatures showed longer breakthrough times. This fact suggests that the H_2S capture capacity of Cu-ETS-2 becomes larger at higher temperature.

The experimental data were first fitted with the linear fixed-bed adsorption model or "The Transport Equation" (Eq. (5)). This model considers only an adsorption interaction without including any chemical reaction term. Figure 4(a) shows the best fit of experimental data at 25 °C by using the "The Transport Equation." This model is less than perfect in fitting the experimental data. The main issue resides in describing the "dispersion effect" of the front during the breakthrough lapse. The model resolution provides simulated breakthrough profiles much sharper than those obtained from experiments.

Then, the experimental data were fitted using the model defined by Eq. (9) which includes a chemical reaction term (Fig. 4(b)). The comparison of Figures 4(a) and (b) shows that the model including the reaction term (Eq. (9)) better describes the eluting concentration front at the bed outlet. In contrast, the adsorption model without chemical reaction (Eq. (5)) provides a sharp concentration front which is not representative of the H_2S breakthrough profile obtained using a packed-bed of Cu-ETS-2 material. The observed concentration fronts in these experiments showed "dispersion effects" which can be attributed to the chemical reaction step between H_2S molecules and the copper sites. The chemisorption model was able to fit the experimental data successfully pointing out the importance of the chemical reaction step in the model formulation.

Figures 4(c) and (d) show the 3D plots, (i.e., H_2S concentration in ppm vs. bed length z axis and time) corresponding to the results of the numerical resolution of Eqs. (5) and (9) respectively. A sharp concentration front is shown for the case when no chemical reaction is considered (Eq. (5)). On the contrary, a concentration front presenting a higher "dispersion effect" was obtained through the numerical solution of Eq. (9) where a reaction term was included.

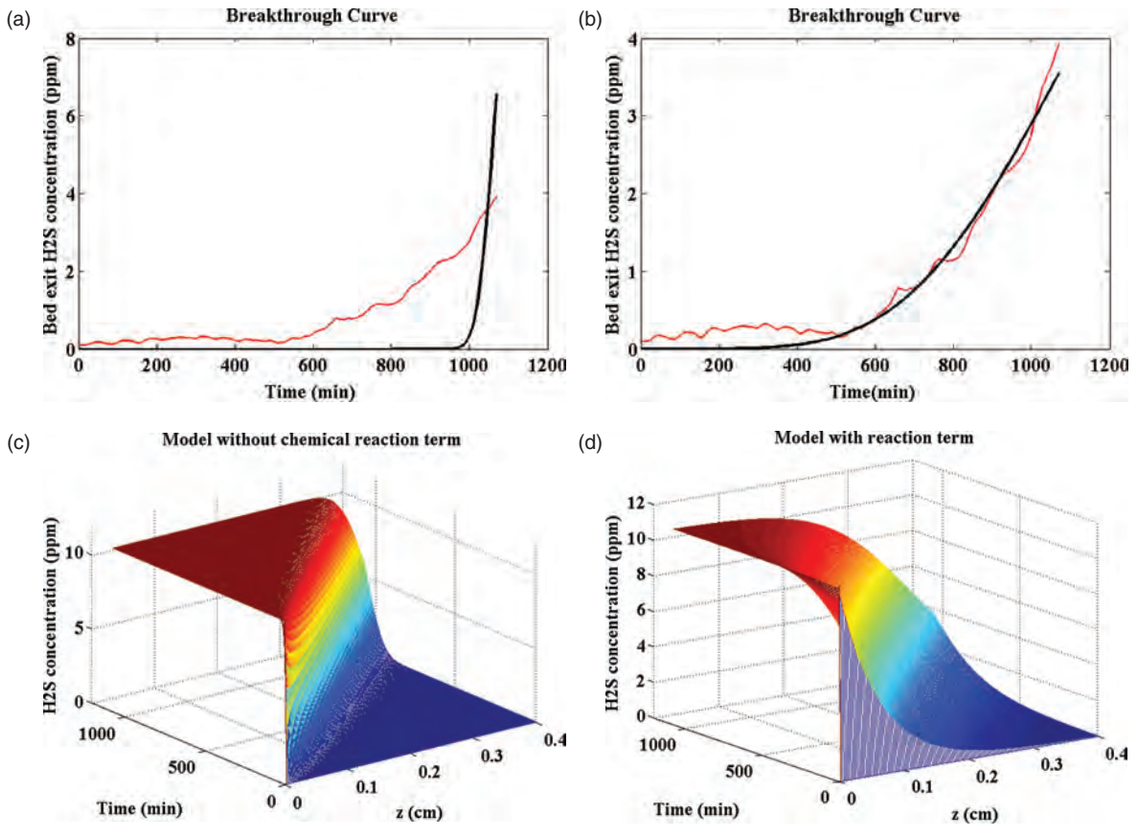

Figure 4. The experimental data at 25 °C fitted by Eq. (5) (a), Eq. (9) (b). The 3D plots of concentration change with time along the bed at 25 °C, Eq. (5) (c) and Eq. (9) (d).

The fitted parameters based on the model of Eqs. (5) and (9) are given in Table II. Even though the transport equation cannot provide a thorough description of each curve at an individual temperature, however, the fit of the entire data set at different temperatures resulted in an increase of k_H parameter magnitudes as temperature increases. The increase trend of the fitted parameter k_H suggests a higher affinity of Cu-ETS-2 material for H_2S at higher temperature, which is an indication of temperature activated chemisorption rather than physisorption. As temperature increased from 25 °C to 250 °C, the k_H value (represents the magnitude of the chemisorption interaction of H_2S molecule and the copper sites) also increased. This is consistent with the trend obtained for the k_H values using the "Transport Equation" model without reaction. The reaction or kinetics parameter K also increased between 25 °C and 150 °C. However, it decreased between 150 °C and 250 °C. As temperature increased from 150 °C to 250 °C, possibly the sulfidation reaction was moderated due to the reduction of active sites as the resulting sulfide covered the active surface. The deactivation parameter (k_d) follows an expected trend. At 250 °C with the highest H_2S capture capacity, Cu-ETS-2 has the lowest k_d which means it takes longer for the adsorbent to get deactivated at this temperature. Thus, when adsorption capacity is higher, adsorbent deactivates slower (lower k_d).

Table II. Fitted parameters for models presented in Eqs. (5) and (9) at 25 °C, 100 °C and 250 °C.

	Eq. (5)	Eq. (9)		
Temperature [°C]	$k_H * 10^{-6}$ [cm^3/g]	$K * 10^{-4}$ [$cm^3/min \cdot g$]	$k_H * 10^{-6}$ [cm^3/g]	$k_d * 10^3$ [ ]
25	5.36	5.56	1.73	3
150	9.6	16	3.04	2.9
250	19.5	9.39	6.5	1.45

3.3.2. *Numerical versus Analytical Resolution for the Proposed Model*

Using method of characteristics, the proposed model given in Eq. (9) can also be solved analytically as:

$$c = c_o \left\{ e^{k/k_d \cdot e^{-k_d}[1-e^{k_d \propto z/v}]} \right\} \tag{10}$$

where

$$\propto = \frac{\varepsilon_b + p_b k_H}{\varepsilon_b}$$

Results show excellent agreement between the breakthrough curves using the analytical solution of the proposed model (Eq. (9)) versus the numerical solution (Eq. (16)), which provides confidence about the simulation results.

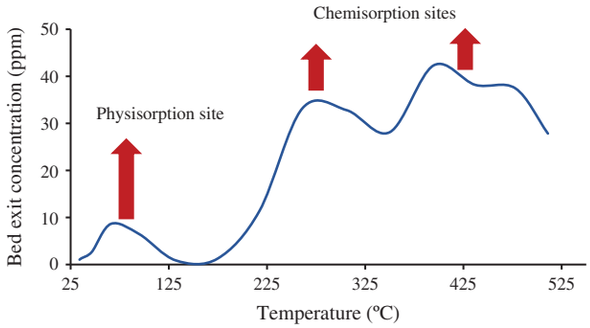

Figure 5. Temperature program desorption curve of H_2S under He with the heating rate of 10 °C/min.

3.3.3. *Desorption Experiments of H_2S on Spent Cu-ETS-2*

Figure 5 shows the profile corresponding to the temperature programmed desorption of H_2S from Cu-ETS-2 sample which was previously saturated at room temperature. The maximum temperature of 500 °C is selected to prevent H_2S decomposition. It has also been reported that hydrogen sulfide decomposition is a highly endothermic process ($\Delta H_{298} = 20.25$ kcal/mol) at temperatures below 527 °C and its total conversion does not exceed 1.5–2%.[49]

As temperature increases, H_2S molecules are desorbed and form the desorption peaks at different temperatures. This indicates that there are adsorption sites with different interaction energies on the surface of Cu-ETS-2.[50] The small peak below 150 °C could be assigned to the low energy interaction sites associated with physisorption sites on the solid.

Previous reports[18–20, 22] showed that H_2S adsorption on metallic Cu and copper oxide is accompanied by dissociation and mainly interacts with the metal centers of the oxides,[24] which proceeds by two stepwise reactions:

$$\mathrm{Cu} + \mathrm{H_2S_g} \underset{\text{Molecular adsorption}}{\longrightarrow} \{\mathrm{Cu-SH_{2\,ads}}\}$$

$$\underset{\text{Dissociative adsorption}}{\longrightarrow} \{(\mathrm{Cu-SH})_{\mathrm{ads}} + \mathrm{H_{ads}}\}$$

These steps occur spontaneously and continue by second hydrogen separation and further metal sulfide formation step.[26] TiO_2 surface, on the other hand, promotes H_2S dissociation according to the large Bronsted acid-base reaction.[25] Thus, at room temperature H_2S strongly adsorbs and disassociates on the Cu-ETS-2 surface; mostly on metal active sites or very little on the titanate substrate.

H_2S molecules chemisorbed on copper sites requires more energy for desorption and they start to desorb at higher temperatures than 150 °C. The presence of consecutive peaks as the desorption temperature increases from 150 °C up to 500 °C suggests that copper sites on the surface provide different energy interactions and chemisorption is a key interaction in the process.

4. CONCLUSIONS

Diluted H_2S breakthrough experiments through a packed bed of Cu-ETS-2 adsorbent were modeled applying the continuity equation to the system by taking into account the characteristics of the adsorbent material. The increase of the H_2S breakthrough times as the experimental temperature increased can be explained by the growing chemisorption interaction as temperature rose from 25 °C to 250 °C. This was also consistent with the temperature programmed desorption experiments which showed desorption peaks of larger magnitudes at temperatures higher than 200 °C. A fixed bed model with reaction term was able to fit the experimental data as well and it could partially explain the breakthrough profiles behavior through the increasing reaction kinetics with temperature.

NOMENCLATURE

a	Deactivation rate term
b	Langmuir equilibrium constant
c	Concentration in fluid phase
d_p	Particle diameter
d_b	Bed internal diameter
K	Kinetic parameter
k_d	Deactivation constant
k_f	Mass transfer coefficient
k_H	Henry's constant
k_r	Reaction rate constant
L_b	Adsorbent bed length
P	Gas-phase pressure
dP	Pressure drop
Q	Gas flowrate
q	Concentration in solid phase
T	Temperature
t	Time
w	Adsorbent weight
z	Distance.

Greek Letters

ε_b	Bed void fraction
θ	Surface coverage
ρ_b	Bed density
μ	Viscosity
v	Interstitial fluid velocity.

Acknowledgments: The authors would like to express heartfelt thanks to Tong Qiu and Weizhu An for help with experimental set-up. Financial support from the Helmholtz-Alberta Initiative and the Canada Research Chair in Molecular Sieve Nanomaterials (Steven M. Kuznicki) is gratefully appreciated.

References and Notes

1. C. Babé, M. Tayakout-Fayolle, C. Geantet, M. Vrinat, G. Bergeret, T. Huard, and D. Bazer-Bachi, *Chemical Engineering Science* 82, 73 (**2012**).

2. N. M. Hieu, H. Kim, C. Kim, S.-K. Hong, and D. Kim, *J. Nanosci. Nanotechnol.* 16, 10351 (**2016**).
3. M. Xue, R. Chitrakar, K. Sakane, and K. Ooi, *Green Chemistry* 5, 529 (**2003**).
4. S. Jeong and D. H. Kim, *J. Nanosci. Nanotechnol.* 16, 441 (**2016**).
5. C. L. Carnes and K. J. Klabunde, *Chemistry of Materials* 14, 1806 (**2002**).
6. A. Katoch, J.-H. Kim, and S. S. Kim, *J. Nanosci. Nanotechnol.* 15, 8637 (**2015**).
7. D. Melo, J. de Souza, M. Melo, A. Martinelli, G. Cachima, and J. Cunha, *Colloids and Surfaces A: Physicochemical and Engineering Aspects* 272, 32 (**2006**).
8. D. Crespo, G. Qi, Y. Wang, F. H. Yang, and R. T. Yang, *Industrial and Engineering Chemistry Research* 47, 1238 (**2008**).
9. P. Kumar, C. Sung, O. Muraza, M. Cococcioni, S. Al Hashimi, A. McCormick, and M. Tsapatsis, *Microporous and Mesoporous Materials* 146, 127 (**2011**).
10. D. Nguyen-Thanh and T. Bandosz, *Carbon* 43, 359 (**2005**).
11. F. Li, J. Wei, Y. Yang, G. H. Yang, and T. Lei, *Applied Mechanics and Materials* 475, 1329 (**2014**).
12. Q. Xue and Y. Liu, *Journal of Industrial and Engineering Chemistry* 18, 169 (**2012**).
13. M. Hussain, N. Abbas, D. Fino, and N. Russo, *Chemical Engineering Journal* 188, 222 (**2012**).
14. X. Wang, T. Sun, J. Yang, L. Zhao, and J. Jia, *Chemical Engineering Journal* 142, 48 (**2008**).
15. D. Montes, E. Tocuyo, E. Gonzaĺez, D. Rodriǵuez, R. Solano, R. Atencio, M. A. Ramos, and A. Moronta, *Microporous and Mesoporous Materials* 168, 111 (**2013**).
16. S. Rezaei, A. Tavana, J. A. Sawada, L. Wu, A. S. M. Junaid, and S. M. Kuznicki, *Industrial and Engineering Chemistry Research* 51, 12430 (**2012**).
17. S. Rezaei, M. O. D. Jarligo, L. Wu, and S. M. Kuznicki, *Chem. Engi. Sci.* 123, 444 (**2015**).
18. A. N. Startsev, I. I. Zakharov, O. V. Voroshina, A. V. Pashigreva, and V. N. Parmon, *Doklady Physical Chemistry* 399, 283 (**2004**).
19. Y. M. Choi, C. Compson, M. C. Lin, and M. Liu, *Chem. Phys.Lett.* 421, 179 (**2006**).
20. I. I. Zakharov, A. N. Startsev, O. V. Voroshina, A. V. Pashigreva, N. A. Chashkova, and V. N. Parmon, *Russian Journal of Physical Chemistry A* 80, 1403 (**2006**).
21. D. R. Alfonso, *Surface Science* 602, 2758 (**2008**).
22. Q. L. Tang, S. R. Zhang, and Y. P. Liang, *J. Phys. Chem. C* 116, 20321 (**2012**).
23. S. H. Chen, S. Q. Sun, B. J. Lian, Y. F. Ma, Y. G. Yan, and S. Q. Hu, *Surf. Sci.* 620, 51 (**2014**).
24. J. A. Rodriguez, S. Chaturvedi, M. Kuhn, and J. Hrbek, *J. Phys. Chem. B* 5511 (**1998**).
25. A. Fahmi, J. Ahdjoudj, and C. Minot, *Surf. Sci.* 352–354, 529 (**1996**).
26. J. Sun, S. Modi, K. Liu, R. Lesieur, and J. Buglass, *Energy Fuels* 21, 1863 (**2007**).
27. S. Guntuka, S. Farooq, and A. Rajendran, *Industrial and Engineering Chemistry Research* 47, 163 (**2008**).
28. Y. Xiao, S. Wang, D. Wu, and Q. Yuan, *Journal of Hazardous Materials* 153, 1193 (**2008**).
29. S. N. Nobar and S. Farooq, *Chem. Engi. Sci.* 801 (**2012**).
30. R. Haghpanah, A. Rajendran, S. Farooq, I. A. Karimi, and M. Amanullah, *Industrial and Engineering Chemistry Research* 51, 14834 (**2012**).
31. K. B. Lee, A. Verdooren, H. S. Caram, and S. Sircar, *J. Coll. Inter. Sci.* 308, 30 (**2007**).
32. O. Levenspiel, Chemical Reaction Engineering; An Introduction to the Design of Chemical Reactors, Wiley, New York (**1962**).
33. C. H. Bartholomew, *Applied Catalysis A: General* 212, 17 (**2001**).
34. T. Doğu, *Chemical Engineering Journal* 21, 213 (**1981**).
35. N. Yaşyerli, T. Doğu, G. Doğu, and I. Ar, *Chem. Engi. Sci.* 51, 2523 (**1996**).
36. Y. Suyadal, M. Erol, and H. Oguz, *Industrial and Engineering Chemistry Research* 39, 724 (**2000**).
37. S. Yasyerli, G. Dogu, I. Ar, and T. Dogu, *Industrial and Engineering Chemistry Research* 40, 5206 (**2001**).
38. S. Yasyerli, I. Ar, G. Dogu, and T. Dogu, *Chemical Engineering and Processing: Process Intensification* 41, 785 (**2002**).
39. S. Yasyerli, G. Dogu, I. Ar, and T. Dogu, *Chemical Engineering Communications* 190, 1055 (**2003**).
40. T. Kopac and S. Kocabas, *Advances in Environmental Research* 8, 417 (**2004**).
41. H. F. Garces, H. M. Galindo, L. J. Garces, J. Hunt, A. Morey, and S. L. Suib, *Microporous and Mesoporous Materials* 127, 190 (**2010**).
42. T. Ko and H. Hsueh, *Aerosol and Air Quality Research* 12, 1355 (**2012**).
43. K. J. Leary, J. N. Michaels, and A. M. Stacy, *American Institute of Chemical Engineers Journal* 34, 263 (**1988**).
44. A. M. de Jong and J. W. Niemantsverdriet, *Surf. Sci.* 233, 355 (**1990**).
45. K. Kočí, P. Praus, M. Edelmannová, N. Ambrožová, I. Troppová, D. Fridrichová, G. Słowik, and J. Ryczkowski, *J. Nanosci. Nanotechnol.* 17, 4041 (**2017**).
46. T. Meng, D. Mao, Q. Guo, and Z. Ma, *J. Nanosci. Nanotechnol.* 17, 3779 (**2017**).
47. R. Haghpanah, A. Majumder, R. Nilam, A. Rajendran, S. Farooq, I. A. Karimi, and M. Amanullah, *Industrial and Engineering Chemistry Research* 52, 4249 (**2013**).
48. R. B. Bird, W. E. Stewart, and E. N. Lightfoot, Transport Phenomena, Second edn., Wiley (**2006**).
49. A. Startsev, O. Kruglyakova, Y. Chesalov, S. Ruzankin, E. Kravtsov, T. Larina, and E. Paukshtis, *Topics in Catalysis* 56, 969 (**2013**).
50. K. J. Leary, J. N. Michaels, and A. M. Stacy, *American Institute of Chemical Engineers Journal* 34, 263 (**1988**).

Received: 18 July 2017. Accepted: 5 January 2018.